

Geometric implicit neural representations for signed distance functions

Luiz Schirmer* Tiago Novello Vinícius da Silva Guilherme Schardong
 Daniel Perazzo Hélio Lopes Nuno Gonçalves Luiz Velho

November 11, 2025

Abstract

Implicit neural representations (INRs) have emerged as a promising framework for representing signals in low-dimensional spaces. This survey reviews the existing literature on the specialized INR problem of approximating *signed distance functions* (SDFs) for surface scenes, using either oriented point clouds or a set of posed images. We refer to neural SDFs that incorporate differential geometry tools, such as normals and curvatures, in their loss functions as *geometric INRs*. The key idea behind this 3D reconstruction approach is to include additional *regularization* terms in the loss function, ensuring that the INR satisfies certain global properties that the function should hold – such as having unit gradient in the case of SDFs. We explore key methodological components, including the definition of INR, the construction of geometric loss functions, and sampling schemes from a differential geometry perspective. Our review highlights the significant advancements enabled by geometric INRs in surface reconstruction from oriented point clouds and posed images.

Keywords: Neural Fields, Implicit Representations, Differential Geometry

1 Introduction

An *implicit neural representation* (INR) is a *neural network* that parameterizes a signal in a low-dimensional domain. This representation differs from

classical methods, as it encodes the signal implicitly in its parameters by mapping coordinates to target signal values. For example, in the case of an implicit surface, an INR f takes a 3D point p and returns the isosurface value $f(p)$. In this scenario, we aim for the INR to approximate the input data as closely as possible, similar to the problem of approximating signals using *radial basis functions*. INRs provide a compact, high-quality, and smooth approximation for discrete data. Furthermore, INRs allow calculating higher-order derivatives in closed form through automatic differentiation, which is present in modern machine learning frameworks.

INRs are smooth, compact networks that are fast to evaluate and have a high representational capacity. This has motivated their use in several contexts for example: images [4, 38], face morphing [44, 73, 74], signed/unsigned distance functions [37, 34, 46, 20, 49, 61, 45, 5, 8, 42], displacement fields [65], surface animation [29, 35], multiresolution signals [39, 43, 20], occupancy [30], constructive solid geometry [26], radiance fields [31, 41], textures [40], 3D reconstruction from images and videos [58, 59, 19], among others. These works leverage the fact that INRs are compositions of smooth maps to explore their derivatives during training. From these various applications, geometry processing is a noteworthy field with many applications [58, 34, 20, 59].

The parameters θ of an INR f are *implicitly* defined as the solution to a non-linear equation $\mathcal{L}(\theta) = 0$, where \mathcal{L} is a *loss function* that ensures f fits the samples $\{p_i, \ell(p_i)\}$ of the ground-truth function ℓ and

*Corresponding author: luiz.schirmer@ufsm.br

satisfies certain properties held by ℓ . For instance, when fitting f to the *signed distance function* (SDF) of a surface, a term is added to the loss function to enforce the gradient ∇f of the network to be unitary; the Eikonal equation $\|\nabla f\| = 1$. This is a fundamental concept in INRs, as SDFs are solutions to this partial differential equation. The primary benefit of adding this constraint is that the sampling $\{p_i, \ell(p_i)\}$ is often sparse and concentrated near the ground-truth surface. Consequently, training f only on these samples could introduce noise in regions with no data. Imposing the Eikonal equation on additional points helps regularizing the INR training.

In a neural SDF f , the output $f(p)$ is a distance value that can be positive or negative, indicating whether a point is inside or outside the underlying compact surface. A distance value of zero indicates that the point lies on the implicit surface S . The gradient $N = \nabla f$ provides the *normal* field of S , and its Hessian $\text{Hess}(f)$, the *shape operator*, gives the curvatures. In this work, we present a survey on *geometric* approaches that explore these differential objects during the training and inference of INRs.

We define a *geometric* INR as a neural network $f : \mathbb{R}^3 \rightarrow \mathbb{R}$ approximating a SDF of a regular surface S , i.e. $\|\nabla f\| \approx 1$, such that its parameters θ are implicitly defined by $\mathcal{L}(\theta) = 0$, with \mathcal{L} enforcing geometrical properties of S through ∇f and $\mathbf{H}f$. To enforce the SDF property, an Eikonal term $\int_{\Omega} (\|\nabla f\| - 1)^2 dp$ is added to \mathcal{L} , where Ω is the training domain. Another important geometric term arises from forcing the alignment of the normals N of S with the gradient ∇f , i.e. $\int_S (1 - \langle \nabla f, N \rangle) dS$.

To bring an in-depth discussion about geometric INRs we consider the following *training pipeline*. It begins with the **input data**, which could be either an oriented point cloud consisting of points and normals sampled from the underlying surface S , or a set of posed images taken from a scene having S as a surface. Next, a **neural network** (INR) $f : \mathbb{R}^3 \rightarrow \mathbb{R}$ with parameters θ is defined to fit the SDF of S . This fitting is achieved through optimization of a **geometric loss function** \mathcal{L} using a variant of the gradient descent algorithm. However, computing the gradient $\nabla \mathcal{L}$ may be infeasible in practice due to the size of the data set. Thus, it is common to consider mini-batches

(**sampling** step) which exploit geometric properties of the underlying surface S to speed up the training. Once the INR f is trained, the SDF properties of f can be leveraged for various applications, such as geometry **inference** using *sphere tracing* or surface evolution using *level-set methods*.

We present recent frameworks that enhance the training performance of INRs by exploring geometrical losses and curvature information to sample points during training. Additionally, we discuss approaches that utilize geometric INRs for 3D reconstruction from posed images, where the neural SDF is used to represent the scene geometry. Finally, we provide examples of dynamic geometric INR approaches for learning surface animation from oriented point clouds and (time-dependent) posed images. To achieve this, the network domain must be extended to space-time $\mathbb{R}^3 \times \mathbb{R}$ to encode the time variable [35, 29].

Terminology In the visual computing community, implicit neural representations have also been referred to as neural fields, neural implicits, and coordinate-based neural networks. In this paper, we focus on the terminology “implicit neural representations” despite some references using the other terms.

The paper is organized as follows. Section 2 discusses the main aspects of implicit surface reconstruction, focusing on the application of the Eikonal equation, oriented point-cloud-based reconstruction and classical image-based approaches. Section 3 shows a geometric framework to solve the geometric implicit neural representation problem, where we detail the input data, loss function details, and dataset sampling. Section 4 presents applications considered state-of-the-art for INRs, where we focus on neural implicit surface reconstruction from images, from oriented point clouds, multi-resolution, and dynamic INRs with applications for deforming objects and animation. The final remarks are drawn at the conclusion in Section 5.

2 Implicit surface reconstruction

Implicit representations are commonly used in computer graphics to represent 3D shapes. Unlike explicit representations (e.g. using triangle meshes) implicit representations encode a surface S as the zero-level set of a function $f : \mathbb{R}^3 \rightarrow \mathbb{R}$. For the surface S to be regular, the zero must be a regular value of f , that is, $\nabla f \neq 0$ on $S = f^{-1}(0)$. Again, SDFs are a common example of an implicit representation, where f is the solution of the Eikonal equation:

$$\|\nabla f\| = 1 \text{ subject to } f = 0 \text{ on } S. \quad (1)$$

In this work, we present recent strategies to solve (1) by parameterizing f with an INR $f : \mathbb{R}^3 \rightarrow \mathbb{R}$, with parameters θ . To approximate a solution of this equation, it is common to define a loss function \mathcal{L} to enforce f to be a solution. Solving this equation reveals that $\langle \nabla f, N \rangle = 1$ on S , indicating that ∇f aligns with the normals N of S . We refer to a solution of the above problem as a *geometric INR*.

Before presenting examples of training pipelines for geometric INRs, we recall some classic approaches.

2.1 Oriented point cloud based reconstruction

Radial basis functions (RBFs) [3] is a classical method that can be used to approximate the SDF of a surface S from a sample $\{p_i, f_i\}$ of this function. The RBF is expressed as $s(p) = \sum \lambda_i \phi(\|p - p_i\|)$, where the coefficients $\lambda_i \in \mathbb{R}$ are determined by imposing $s(p_i) = f_i$. The *radial function* $\phi : \mathbb{R}^+ \rightarrow \mathbb{R}$ is a real function and p_i are the centers of the RBF [34]. Note that the RBF representation depends on the data since its interpolant s depends on the input points p_i .

Poisson surface reconstruction [16] is another classical method widely used in computer graphics to reconstruct a surface from an oriented point cloud $\{p_i, N_i\}$. It revolves around solving the *Poisson's equation*, using $\{p_i, N_i\}$. The objective is to reconstruct an implicit function f of the underlying

surface by asking it to be zero at p_i and to have gradients at p_i equal to N_i . The pairs $\{p_i, N_i\}$ are used to define a vector field V . Then, f is computed by optimizing $\min_f \|\nabla f - V\|$ which results in a Poisson problem: $\Delta f = \nabla \cdot V$.

2.2 Image-based reconstruction

There are many classical works that aim to reconstruct the surface S of a 3D scene from a set of unordered images $\{I_j\}$ [52]. Generally, these methods focus on obtaining an oriented point cloud $\{p_i, N_i\}$ using *structure-from-motion* [57]. The surface S can then be reconstructed using Poisson surface reconstruction [16]. COLMAP [47] is a standard example of this approach. It extracts features from each I_j , e.g., using SIFT [23], and searches for feature correspondences between the images, using RANSAC [9]. Finally, using bundle adjustment, it computes camera positions and the points p_i such that the corresponding viewing rays intersect.

Recently, implicit neural representations initially developed for the novel view synthesis problem such as NeRFs [31] have been gaining popularity for representing these systems. Recently, adaptations for NeRFs have been created for the task of implicit surface reconstruction [58, 59, 63, 21]. We will present this problem in more detail in Subsection 4.2

3 Geometric INR framework

3.1 Overview of the problem

This section presents an overview of the framework used to solve the geometric INR problem of training the parameters θ of an INR $f : \mathbb{R}^3 \rightarrow \mathbb{R}$ to approximate the SDF of a desired surface S . This pipeline describes the problem for both point-based and image-based surface reconstruction. To present this pipeline we follow the scheme in Figure 1.

The **input** can be either a sample of oriented points $\{p_i, N_i\}_{i=1}^n$ from the *ground truth* surface S or a set of posed images $\{\mathcal{I}_j\}$ taken from a scene having S as its surface. The **output** is an INR f approximating the SDF of S . To estimate an SDF with

its zero-level set of S from \mathcal{J}_j , it is assumed that the existence of a projection invertible matrix transformation W_j for each image, mapping from screen to world coordinates. Although the problem seems fundamentally different, we shall discuss their similarities later. The framework explores the normals N to define a loss function and the curvatures of the surface to sample the mini-batches.

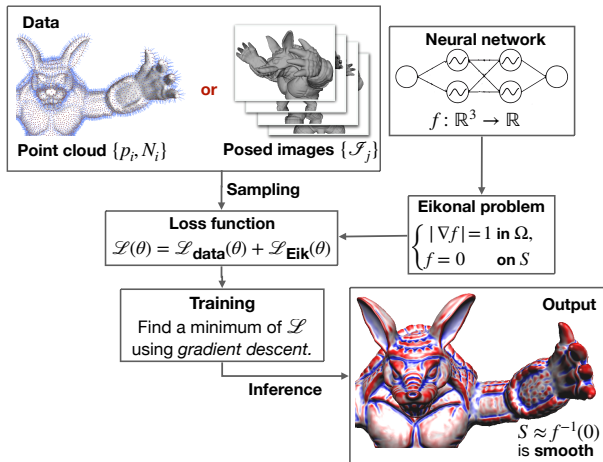


Figure 1: Geometric INR pipeline: The input data can be either an oriented point cloud $\{p_i, N_i\}$ or a set of posed images $\{\mathcal{J}_j\}$. A neural network f is then defined to fit a solution to the Eikonal equation. To train f , we define a loss function consisting of two terms: data constraint and Eikonal constraint. For the point-based data, we simply enforce $f(p_i) = 0$ and $\nabla f(p_i) = N_i$. For the image-based data, we rely on volume rendering techniques. Finally, gradient descent is used to optimize the resulting loss function.

Next, we define a **neural network** (INR) f , with parameters θ , to fit the SDF ℓ of the ground-truth surface S . For this, we define a **loss function** $\mathcal{L} = \mathcal{L}_{\text{data}} + \mathcal{L}_{\text{Eik}}$ to enforce f to be a solution of Eikonal equation (1). The data term $\mathcal{L}_{\text{data}}$ forces f to fit the input data. \mathcal{L}_{Eik} forces f to be a solution of the Eikonal equation; thus, it works like a (implicit) regularization.

For image-based reconstruction, the data term $\mathcal{L}_{\text{data}}$ is modeled using volume rendering [58, 59].

This involves defining a differentiable rendering function $I(\theta, W_j)$ for the camera corresponding to each posed image (\mathcal{J}_j, W_j) . Thus, the data constraint $\mathcal{L}_{\text{data}}$ for training θ is defined by forcing $I(\theta, W_j) = \mathcal{J}_j$. Some techniques also incorporate geometric regularizations, such as curvature-based methods [19], or different approaches to map the SDF to a density-based operator [63].

The **training** step consists of using a variant of the gradient descent algorithm to find a minimum of \mathcal{L} . However, in practice, computing the gradient $\nabla \mathcal{L}(\theta)$ may be unfeasible; thus, we consider **sampling** mini-batches of the input data. Once we have the INR f trained, we can infer its geometry to **render** its zero-level set $f^{-1}(0)$.

The following sections present each component of geometric INR training in detail.

3.2 Input data

Here, we describe the two kinds of data options (input of the pipeline in Figure 1) to reconstruct the surface S .

Oriented point cloud Let $\{p_i, N_i\}_{i=1}^n$ be an oriented point cloud sampled from S , where $p_i \in S$ and N_i are the normals to S at p_i . We aim to reconstruct the SDF ℓ of S by enforcing $f(p_i) = 0$ and $\nabla f(p_i) = N_i$. However, this approach may result in a neural SDF with spurious components on its zero-level set. To mitigate such noise, we sample additional points $\{q_k\}$ outside $\{p_i\}$ to regularize the training. As a result, we obtain a set of points being the union of $\{p_i\}$ and $\{q_k\}$ with their corresponding SDF values.

Posed images For the image-based setting, we assume a set of images \mathcal{J}_j with their corresponding projection matrices W_j . COLMAP [47] is commonly used whenever the projection matrices are unavailable. W_j is the product $K_j \cdot [R_j | t_j]$ of the intrinsic matrix $K_j \in \mathbb{R}^{4 \times 4}$ and the extrinsic matrix $[R_j | t_j]$. The intrinsic matrix K_j includes parameters of the camera, such as focal length and center of projection. The extrinsic matrix $[R_j | t_j]$ consists of the

orthogonal matrix R_j for camera orientation and the camera position $-t_j$. Note that in COLMAP, the images are assumed to have significant overlap, otherwise the feature matching step fails, resulting in poor approximations of W_j .

3.3 Network architecture

We assume the INR $f : \mathbb{R}^3 \rightarrow \mathbb{R}$ to be parametrized by a *multilayer perceptron* (MLP) defined as follows.

$$f(p) = W_n \circ f_{n-1} \circ f_{n-2} \circ \dots \circ f_0(p) + b_n \quad (2)$$

where $f_i(p_i) = \varphi(W_i p_i + b_i)$ is the i th layer, and p_i is the output of f_{i-1} , i.e. $p_i = f_{i-1} \circ \dots \circ f_0(p)$. Here we apply the smooth activation function $\varphi : \mathbb{R} \rightarrow \mathbb{R}$ to each coordinate of the affine map, which is formed by the linear map $W_i : \mathbb{R}^{N_i} \rightarrow \mathbb{R}^{N_{i+1}}$ and the bias $b_i \in \mathbb{R}^{N_{i+1}}$. The operators W_i are represented as matrices, and b_i as vectors, combining their coefficients to form the parameters θ of the function f . In the following section we define a loss function to train θ to fit f to the input data.

The choice of the activation function φ has a great impact on the representation capacity of f . For example, using sines, that is $\varphi = \sin$, results in a powerful INR architecture for surface reconstruction from oriented point clouds [49, 34].

For image-based reconstruction, it is common to use Fourier feature mapping [54] to represent the neural SDF [58]. In this approach, the activation function is $\varphi = \text{ReLU}$, and the first layer projects the input onto a list of sines and cosines. However, this method often results in slow training time. To speed up training and rendering times, hashgrid-based representation was proposed in [32, 19, 59].

3.4 Loss function

We now define a loss function \mathcal{L} to train the parameters θ of the INR f . Again, we start with the oriented point-based case.

Oriented point-based rendering We use the input data $\{p_i, N_i\}_{i=1}^n$ sampled from a surface S and the Eikonal equation (1) to define the loss function

\mathcal{L} as the composition of $\mathcal{L}_{\text{data}}$, and \mathcal{L}_{Eik} . This loss is used to optimize θ such that $f : \mathbb{R}^3 \rightarrow \mathbb{R}$ approximates the SDF ℓ of S .

$$\mathcal{L}(\theta) = \underbrace{\frac{1}{n} \sum_i f(p_i)^2 + \left(1 - \langle \nabla f(p_i), N_i \rangle\right)}_{\mathcal{L}_{\text{data}}} + \underbrace{\int_{\Omega} (1 - \|\nabla f\|)^2 dp}_{\mathcal{L}_{\text{Eik}}} \quad (3)$$

Here, \mathcal{L}_{Eik} encourages f to be the SDF of a set \mathcal{X} by ensuring that $\|\nabla f\| = 1$, $\mathcal{L}_{\text{data}}$ encourages \mathcal{X} to contain S ; i.e. $f = \ell$ on $\{p_i\}$. In addition, it asks for the alignment between ∇f and the normals of S to regularize the orientation near the zero-level set.

Typically, an additional term is added to (3) to penalize points outside S , forcing f to be the SDF of S (i.e., $\mathcal{X} = S$) [49]. A common approach is to extend $\mathcal{L}_{\text{data}}$ to consider (off-surface) points outside S by using an approximation of the SDF of S [34]. The SDF approximation at a point p can be computed using $|\ell(p)| \approx \min_i \|p - p_i\|$. The sign of $\ell(p)$ at a specific point p is negative if p lies inside the surface S and positive otherwise. Note that for each point p_i with a normal N_i , the sign of $\langle p - p_i, N_i \rangle$ indicates the side of the tangent plane that p belongs to [34]. Therefore, we can estimate the sign of $\ell(p)$ by adopting the dominant signs of the numbers $\langle p - p_j, N_j \rangle$, with $\{p_j\}$ being a subset of the point cloud.

Image-based rendering The traditional image-based pipeline for surface reconstruction converts the SDF f to a volume density function σ by composing f with a density distribution function ρ , that is, $\sigma = \rho \circ f$. Then, volume rendering is applied to create an image given a camera view. Getting the intensity for a pixel p along a view direction v can be computed using *ray marching*: where we march along a ray $r(t) = o + tv$ and accumulate the colors $c(r(t))$ and densities $\sigma(r(t))$ [15]. The integral is done in the *near* and *far ray* bounds: t_n and t_f . The volume rendering equation is given by:

$$I(r) = \int_{t_n}^{t_f} c(r(t)) \sigma(r(t)) \exp\left(-\int_{t_n}^t \sigma(r(s)) ds\right) dt. \quad (4)$$

To solve (4), most methods discretize the ray and employ numerical methods [27]. This results in a differentiable rendering which allows us to optimize the model parameters θ [31].

After rendering each pixel corresponding to a input image \mathcal{F}_j with projection matrix W_j , we can compare the output image $I(\theta, W_j)$ with its ground-truth \mathcal{F}_j resulting in a *Photometric loss*:

$$\mathcal{L}_{\text{data}}(\theta) = \frac{1}{N} \sum_j^m \|I(\theta, W_j) - \mathcal{F}_j\|^2. \quad (5)$$

3.5 Sampling

Point-based sampling Let $\{p_i, N_i\}_{i=1}^n$ be a sample of the ground-truth surface S . During optimization, we may not be able to compute the gradient $\nabla_{\theta} \mathcal{L}_{\text{data}}(\theta)$ considering the whole dataset. Therefore, it is common to divide it into minibatches. Novello et al. [34] considered the principal curvature information to prioritize regions with more geometric variations of the data during minibatch selection. Regions of higher absolute principal curvatures encode more detailed information than regions with lower absolute curvatures.

Novello et al. [34] proposed splitting $\{p_i\}$ into three sets based on their curvatures: V_1 (low), V_2 (medium), and V_3 (high). During training, they prioritized the points with more geometrical information in V_2 and V_3 while sampling fewer points from V_1 to avoid redundancy. In Figure 2, we can see a comparison between uniform sampling (first row) and this curvature-based sampling (second row). Note how this sampling strategy enhanced convergence during training.

Image-based sampling For the image-based reconstruction case, the sampling for the $\mathcal{L}_{\text{data}}$ term consists of choosing points $\{p_i\}$ along each ray $r(t) = p + tv$, where p is the pixel position and v is the view direction. This approach is used to discretize the volume rendering equation [31]. Most methods follow NeRF, which splits the ray domain interval $[t_n, t_f]$ into evenly spaced times $\{t_i\}$. Then, a time t'_i is uniformly chosen within each interval $[t_i, t_{i+1}]$.

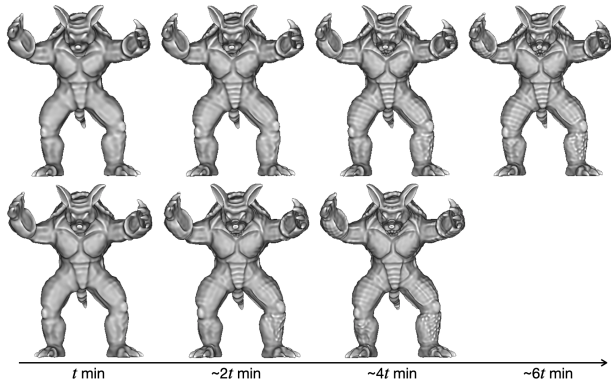


Figure 2: Neural implicit surfaces approximating the Armadillo model. The columns indicate the zero-level sets after 29, 52, 76, and 100 epochs of training. Line 1 shows the results using minibatches sampled uniformly. Line 2 presents the results using the adapted sampling of minibatches with 10% / 70% / 20% of points with low/medium/high features. Image from [34].

There are numerous methods focused on improving the sampling strategy for NeRFs [18, 2].

3.6 Inference

Sphere tracing One important advantage of neural SDFs is in rendering, as we can use the *sphere tracing* algorithm [12]. It approximates the intersection between a ray $r(t) = p_0 + tv$, with p_0 being the starting point, and the zero-level set of a neural SDF f by iterating the system $p_{i+1} = p_i + f(p_i)v$. Note that this requires multiple inferences during rendering. The challenge of operating this algorithm in real-time was addressed in [5]. Figure 3 provides the sphere tracing of the zero-level set of neural SDFs representing the Armadillo and Bunny. The algorithm can accurately ray-cast the surface, avoiding spurious components. Finally, for shading the surface, we compute the normals by simply evaluating the gradient ∇f .

Curvature estimation Another advantage of a neural SDF f is that we can compute the curvatures



Figure 3: Sphere tracing of neural SDFs representing the Armadillo and Bunny models. Both INRs have the same architecture and were trained on the same data during 500 epochs. Image adapted from [34]

of its level sets analytically, as automatic differentiation gives its second partial derivatives. To illustrate an application, consider the input data $\{p_i, N_i\}$ sampled from a triangle mesh representing the underlying surface S . Novello et al. [34] proposed transferring the curvatures of the level sets of f to the vertices of the triangle mesh. In Figure 4, we trained a neural SDF for the Dragon model and calculated the mean curvature using Δf ; blue indicates higher curvatures, and red indicates low curvatures. Additionally, in Figure 5, we show the principal curvatures and directions. The study of discrete curvatures of triangle meshes is a significant topic in discrete differential geometry.

4 Applications for INRs

This section reviews a list of methods and applications of geometric INRs. We divided it in oriented point-cloud methods (Sec. 4.1), Image-based reconstruction (Sec. 4.2), Multiresolution INRs (Sec. 4.3), and Dynamic INRs (Sec. 4.4).

4.1 Surface reconstruction from oriented point clouds

DeepSDF [37] introduced SDFs in the task of representing surfaces as level sets of neural networks.

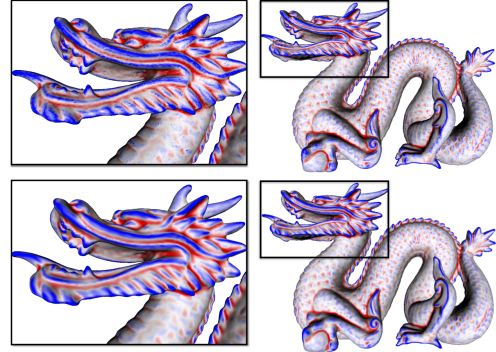


Figure 4: Visual comparison of the discrete and continuous mean curvatures of the Dragon model. The top row shows the discrete mean curvature, while the bottom row shows the mean curvatures computed from the neural SDF using PyTorch framework. Image from [34]

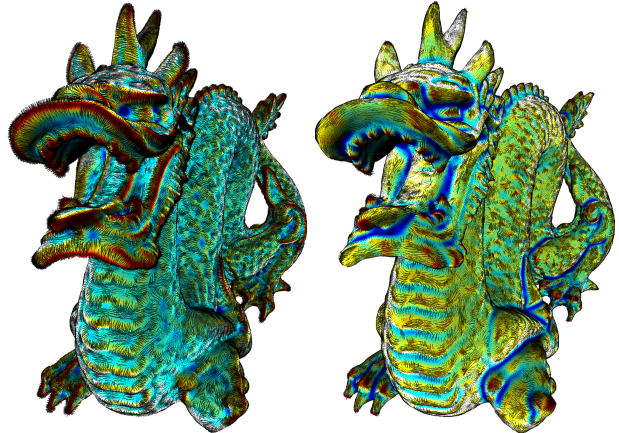


Figure 5: Principal curvatures and directions of the Dragon. Maximal curvatures are shown on the left, while minimal curvatures are on the right. Notice how their directions align nicely with the mesh's ridges and valleys.

However, it does not incorporate any geometric regularization in the loss function, such as enforcing the Eikonal equation (1). Such regularizations were later introduced by IGR [11] and SIREN [49] which represent the underlying surface using a neural INR f and

enforce the Eikonal equation during training. They consider as input an oriented point cloud $\{p_i, N_i\}$, thus, the data term in the loss function simply asks for $f(p_i) = 0$ and $\nabla f(p_i) = N_i$. Figure 6 shows some level sets of MLPs trained using IGR.

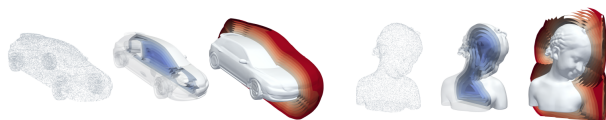


Figure 6: Level sets of MLPs trained with IGR method. Image adapted from [11].

The major difference between IGR and SIREN lies in the architecture of the INR. SIREN proposes parameterizing the INR using a sinusoidal MLP ($\varphi = \sin$ in Equation 2) with an initialization scheme that ensures stability and good convergence during training. Due to their smoothness and large representation capacity, SIRENs have emerged as one of the most popular architectures, influencing many other works in surface representation [34, 51, 14, 8]. Figure 7 shows a surface reconstruction using SIREN to fit an SDF from an oriented point cloud.

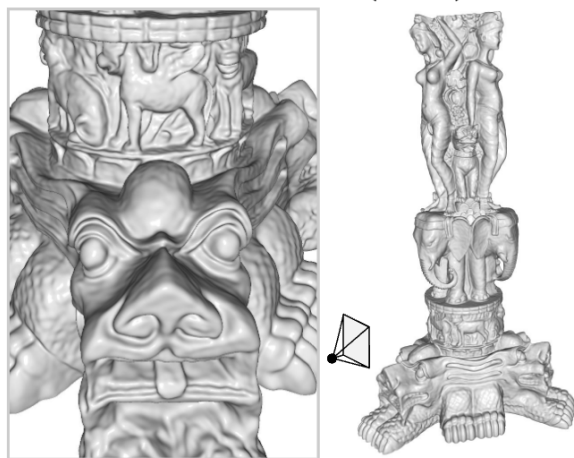


Figure 7: Siren Surface Reconstruction. Figure adapted from [49]

Novello et al. [34] introduced a geometric INR

which explores the curvature of the data during the sampling stage to speed up training by selecting regions with more geometric details. Section 3.5 provide additional details. This method also proposes a loss function that incorporates the curvature of the INR level sets. For this, it uses the closed-form derivatives of the network to estimate differential measures, such as normals and curvatures. This estimation is feasible because the oriented point cloud lies in the neighborhood of the INR zero-level set. Later, Jiao et al. [14] applied this approach to 3D shape reconstruction and analysis of real medical data. They leveraged geometric INRs to create a shape atlas that captures the effects of age, sex, and weight on 3D shapes, enabling shape reconstruction and evolution.

Representing surfaces using SDFs has a common limitation: they can only represent closed surfaces. This is because SDFs inherently assume a clear distinction between the “inside” and “outside” of the underlying surface, making them less suitable for open surfaces. Fainstein et al. [8] addressed this limitation by extending the approach in [34] to open surfaces using *unsigned* distance functions (UDFs).

4.2 Neural Implicit Surface Reconstruction from Images

IDR [62] is one of the first geometric INR approaches to learn a neural SDF from images. IDR simultaneously learns the neural SDF, camera parameters, and a neural renderer that approximates the light reflected from surfaces toward the camera. The geometry is represented as the zero-level set of an MLP, while a neural renderer, based on the rendering equation, implicitly models lighting and materials. Volume SDF [63] adopts a different approach by using *differentiable volume rendering* to optimize the INR parameters. It maps the SDF to a volume density function, assigning a value of 1 to points on the zero-level set and 0 to points far from this set. The neural SDF is optimized through *volume rendering* from the images and is regularized using the Eikonal constraint.

Exploring volume rendering in 3D reconstruction has been motivated by the groundbreaking results of

Neural radiance fields (NeRF) [31, 66, 69, 2]. NeRF employs differentiable volume rendering to optimize the parameters of a ReLU MLP combined with a *Fourier feature mapping* [54]. These networks are trained using volume rendering with supervision from a set of posed images. In this approach, surface geometry is represented as a density function, where the value is 1 for points on the surface and 0 for points far from it. However, surfaces extracted from such neural densities (using marching cubes [22]) tend to be noisy (see Figure 8).

To address the noise issues in NeRF-based surface extraction, Oechsle et al. [36] proposed UNISURF. This method improves the reconstruction quality by replacing NeRF’s density function with an *occupancy network* [30], offering a more robust representation of surface geometry. Figure 8 shows their method evaluated on the DTU dataset Jensen et al. [13].

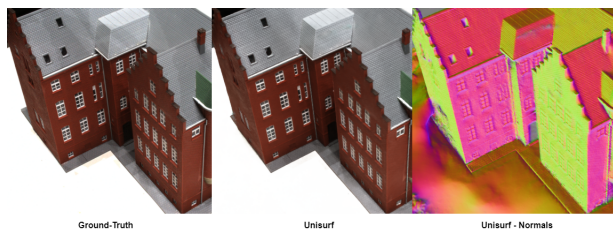


Figure 8: Reconstruction of scan 24 of DTU dataset evaluated with UNISURF.

However, UNISURF does not leverage Eikonal regularization because its underlying model is not an SDF. To our knowledge, NeuS [58] is the first geometric INR method to adapt the NeRF pipeline for training neural SDFs from posed images. It employs a density distribution function (see Sec 3.4) to map SDF values to density values.

NeuS motivated several techniques, addressing aspects such as incorporating depth maps [68], handling sparse views [21], baking the neural SDF [64], enhancing gradient consistency [24], patch warping (NeuralWarp) [6], and applying curvature regularization (Neuralangelo) [19]. Figure 9 shows results from NeuS on the room scene from the dataset presented by Azinović et al. [1].

Neural RGB-D Surface Reconstruction [1] presents

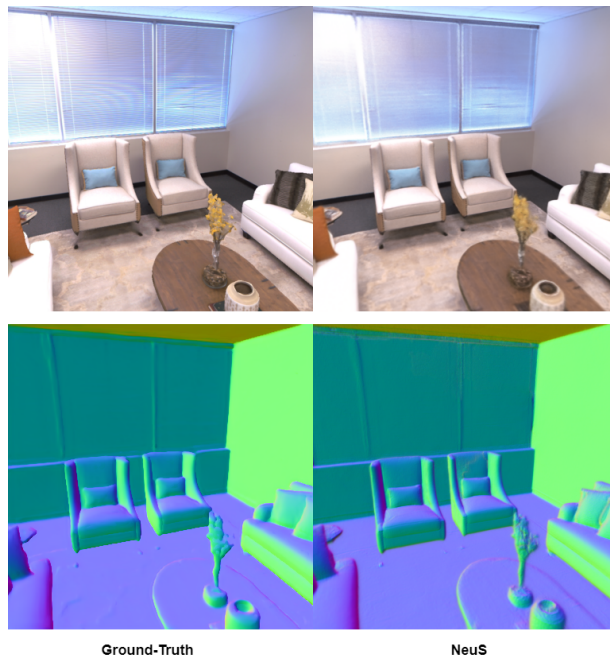


Figure 9: Results from NeuS on the Room scene from the dataset available in the paper Neural RGB-D Surface Reconstruction[1]. The figure shows the scene reconstruction as well as the normal map in comparison to the input data. In these experiments, we ran the NeuS method with its default settings for 20,000 steps.

a method for 3D scene reconstruction that effectively combines RGB and depth data using a hybrid scene representation based on a truncated signed distance function (TSDF) and a volumetric radiance field. The authors address limitations of traditional methods that struggle with noisy depth measurements and incomplete geometry by leveraging color information to fill in gaps where depth data is lacking. Their approach not only improves the quality of geometry reconstructions but also optimizes camera poses to reduce misalignment artifacts, demonstrating superior performance compared to methods like NeRF, NeuS and UNISURF with depth constraints, particularly in complex indoor environments.

Next, NeuS2 [59] and InstantNSR [72] used the

the hashgrid-based network architecture of instant-NGP [32] to make training and rendering faster. In the same vein, Neuralangelo [19] also uses hashgrids mixed with finite gradients methods to make training have a much better performance. Figure 10 presents an overview of the NeuS2 architecture.

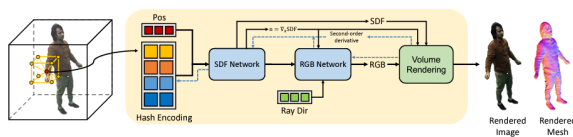


Figure 10: Given a point p , NeuS2 combine its feature from a hashgrid with its coordinates as the input for the neural SDF, which also outputs geometric features. These are subsequently combined with the viewing direction and fed into a RGB network to produce the color value. Figure adapted from [59].

Table 1, shows a comparison between some techniques on the scene 122 of DTU dataset, both in the view synthesis task and the geometry reconstruction. Neuralangelo [19] is, currently, the state-of-the-art in both tasks. It is a example of geometric INR since it parameterizes the underlying surface as a neural SDF and includes the mean curvature of the level sets as a regularizer. The tests were conducted on a computer with an AMD Ryzen 7 5700 CPU, 32 GB of RAM, and an NVIDIA RTX 3080 graphics card. Figure 11 shows a qualitative evaluation with Neuralangelo using the Tanks and Temples dataset[17].



Figure 11: Qualitative comparison on Tanks and Temples dataset[17].

Other than NeuS2, other techniques tried to improve the speed of these representations. For example, MARF [51] introduce the Medial Atom Ray

Method	Mean PSNR (\uparrow)	Chamfer dist. (\downarrow)
NeuS	30.1	0.56
VolSDF	30.38	0.58
UNISURF	27.32	0.66
Neuralangelo	34.91	0.45

Table 1: Performance of Neural SDF methods on the scene 122 of DTU dataset. The PSNR measures the quality of the synthesized view while the Chamfer distance measures the quality of the geometry of the SDF by computing the Chamfer distance for the synthesized mesh.

Fields, a neural object representation enabling differentiable surface rendering with a single network evaluation per camera ray. MARFs address challenges like multi-view consistency and surface discontinuities by using a medial shape representation, offering cost-effective geometrically grounded surface normals and analytical curvature computation. They map camera rays to multiple medial intersection candidates and demonstrate applicability in sub-surface scattering, part segmentation, and representing articulated shapes. With the ability to learn shape priors, MARFs hold promise for tasks like shape retrieval and completion.

Recent research on recovering scene properties from images often employ neural SDFs and differential geometry, with deep neural networks demonstrating inverse rendering of indoor scenes from a single image. However, these methods typically yield coarse lighting representations and lack fine environmental details. Approaches like Lighthouse [50] and NeRFFactor [71] train on natural illumination maps to address environment estimation challenges. PANDORA [7] and RefNeRF utilize multi-view reflections but assume a distant environment modeled with a flat 2D map, while PhySG [70] models surfaces as SDFs for multi-view image rendering. ORCa [56], building on Novello et al. [34]’s concepts, uses reflections on glossy objects to capture hidden environmental information by converting these objects into radiance-field cameras. This transforms object surfaces into virtual sensors, capturing reflections as 2D projections of the

5D environment radiance field. This technique enables depth and radiance estimation, novel-view synthesis beyond the field of view, and imaging around occluders, using differential geometry to estimate curvature for neural implicit surfaces. Figure 12 shows the results of this method and a diagram of its architecture.

To test these different types of SDF reconstruction techniques, and inspired by nerfstudio [55], Yu et al. [67] created SDFStudio, a platform that allows the testing and prototyping of different SDF extraction techniques from images. Table 4.2 show a comparison between the methods, following the input, geometry regularization methods employed.

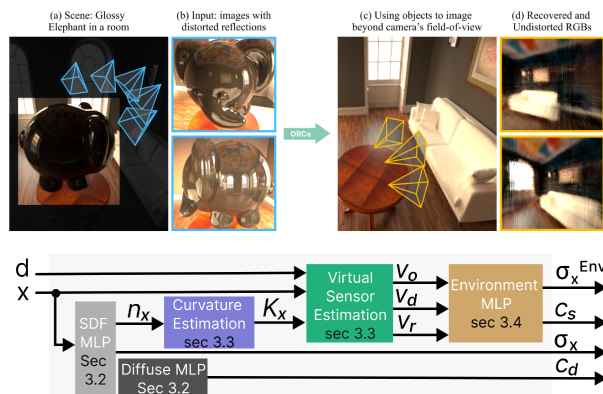


Figure 12: The diagram presents results from the ORCa model and its inputs. It converts objects with unknown geometry into radiance-field cameras by modeling multi-view reflections as projections of a 5D radiance field. Additionally, it transforms the object surface into a virtual sensor to capture this radiance field, enabling depth and radiance estimation of the surrounding environment. The model then queries this radiance field to perform novel view synthesis beyond the field-of-view. ORCa consists of three steps: modeling the object’s geometry as a neural implicit surface, converting the object’s surface into a virtual sensor, and projecting the environment’s radiance field along these virtual cones. The learned radiance field of the environment allows visualization of occluded areas in novel viewpoints. Figure adapted from [56].

4.3 Multiresolution INRs

Multiresolution is a well-studied concept in classical geometry processing [28]. Given this, and inspired by traditional multi-resolution theory for images [60, 25], Lindell et al. [20] introduce BACON, an architecture aimed at addressing the confinement to single-scale signal representation for coordinate-based networks. BACON proposes the creation of an analytical Fourier spectrum, enabling controlled behavior at unsupervised points and allowing for design driven by the signal of spectral characteristics. This method also supports multiscale signal representation without needing supervision at every scale. It has been applied to the neural representation of images, radiance fields, and 3D scenes using SDFs, demonstrating its effectiveness in representing signals across various scales. Figure 13 shows an overview of the method.

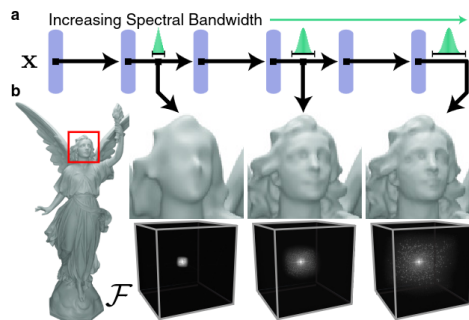


Figure 13: The BACON architecture generates intermediate results with a specific spectral bandwidth chosen during initialization. When trained with high-resolution data, the network learns to decompose outputs across multiple resolutions, useful for tasks like fitting 3D shapes using signed distance functions. The characteristics of the network are defined by its Fourier spectrum, ensuring constrained behavior even in unsupervised scenarios. Figure adapted from [20].

In addressing the limitations of BACON, it is noted that its cut-off of the Fourier spectrum introduces artifacts, particularly the ringing effect observed in images and noise on surfaces. This limitation stems from the inherent constraints of band-limiting, which,

Method	Input	Geometric regularization
PANDORA [7]	Multi-view and polarized RGB	Eikonal Constraint
PhySG [70]	Multi-View RGB	Eikonal Constraint
ORCa [56]	Multi-View RGB	Eikonal Constraint, Mean Curvature Constraint
NeuS [58]	Multi-View RGB	Eikonal Constraint,
NeuS2 [59]	Multi-View RGB	Eikonal Constraint
Neuralangelo [19]	Multi-View RGB	Eikonal Constraint, Mean Curvature
Neural Warp [6]	Multi-View RGB	Eikonal Constraint
Geo-NeuS [10]	Multi-View RGB	Eikonal Constraint
VolSDF [63]	Multi-View RGB	Eikonal Constraint
MonoSDF [68]	Multi-View RGB, Depth/Normals	Eikonal Constraint, Monocular Supervision

Table 2: Breakdown of SDF Reconstruction from multi-view images. We classify them based on the type of input and geometric regularization approaches.

while facilitating certain advantages in signal representation, can also result in undesirable visual artifacts that affect the quality of the output in applications involving high-frequency detail. Other techniques such as BANF [48], build on BACON, but does so with filtering during optimization, which allows it to have a band-limited frequency decomposition. This allows our application of SDF, to have an SDF in multiple levels of detail.

Other techniques allow numerous level-of-detail for rendering different images, for example Takikawa et al. [53], allow for rendering in multiple levels-of-detail and MINER [43] allows the training on multiple levels of scale.

4.4 Dynamic INRs

INRs serve as efficient and versatile geometry representations, encoding both functional and differential data of the underlying object compactly. However, they lack intuitive control over shape editing and animations. Here we explore methods to manipulate implicit surfaces by deformations, whether rigid or not, shape interpolation, and animations. We also list interesting examples of works that do not strictly fit the definition of INR, but exploit differential properties of smooth networks in their objective function.

Niemeyer et al. [33] presents the first approach to leverage deep learning for 3D surface animation. *Oc-*

cupancy flow extends Occupancy Networks [30] by learning a vector field in addition to the occupancy for each point in R^3 continuously along time, thus animating objects in the scene. Their work achieves good results without discretizations and shape templates, both usual techniques incorporated in most contemporaneous methods. More recently Yang et al. [61] proposed to leverage INRs for geometry processing tasks, specifically smoothing and sharpening, in addition to more complicated rigid deformations, such as twists and bends. The authors do not propose their method for animation specifically, but geometrical deformations, thus we classify them under the umbrella of dynamic INRs. The authors propose approximating a local surface of a level set by utilizing the derivatives of the underlying field. By solely relying on the field derivatives, it is possible to use intrinsic geometric properties of the level set, such as curvatures. This enables the construction of loss functions that capture surface priors like elasticity or rigidity. This is made possible by exploiting the inherent infinite differentiability of specific neural fields which facilitates the optimization of loss functions involving higher-order derivatives through gradient descent methods. Consequently, unlike mesh-based geometry processing algorithms that rely on surface discretizations to approximate these objectives, this strategy can directly optimize the derivatives of the field. Their method can apply transformation like

rotation or translation on complex 3D objects as we can see in Figure 14.



Figure 14: Deformation results from Yang et al. [61]: (A) Input shape, (B) Baseline and (C) their method. Their method applies multiple transformation on the Armadillo. Figure adapted from [61].

Similarly to Yang et al. [61], Mehta et al. [29] proposes the use of sinusoidal MLPs to apply smooth deformations, smoothing, and sharpening to surfaces parameterized as INRs. However, as in Yang et al. [61] they still need supervision during the intermediate time-steps to learn a deformation of the base surface. This supervision is done by converting the implicit object to an explicit representation via marching cubes. While their work achieves good results, it does not achieve smoothness along time, since each time-step irreversibly modifies the INR, making it impossible to walk through the deformation after training.

Novello et al. [35] proposes to incorporate the differential equation directly into the loss function, thus removing the need for intermediate-time discretizations. As in [33], Novello et al. [35] expands the domain to include the time parameter ($f : \mathbb{R}^3 \times \mathbb{R} \rightarrow \mathbb{R}$ instead of $f : \mathbb{R}^3 \rightarrow \mathbb{R}$), resulting in a smooth representation in both space and time. The authors proposed to leverage the Mean Curvature Flow for smoothing and sharpening of the base INR, similarly to [61] and [29] as we can see in Figure 15.

Additionally, they propose to exploit the Level Set equation for shape interpolation, as in [29], achieving fully continuous deformations parameterized by a single neural network. See Fig. 16 for interpolation and deformation examples.

An interesting application of dynamic INRs is on the face-morphing task, where the goal is to create a transition between two or more existing faces, or

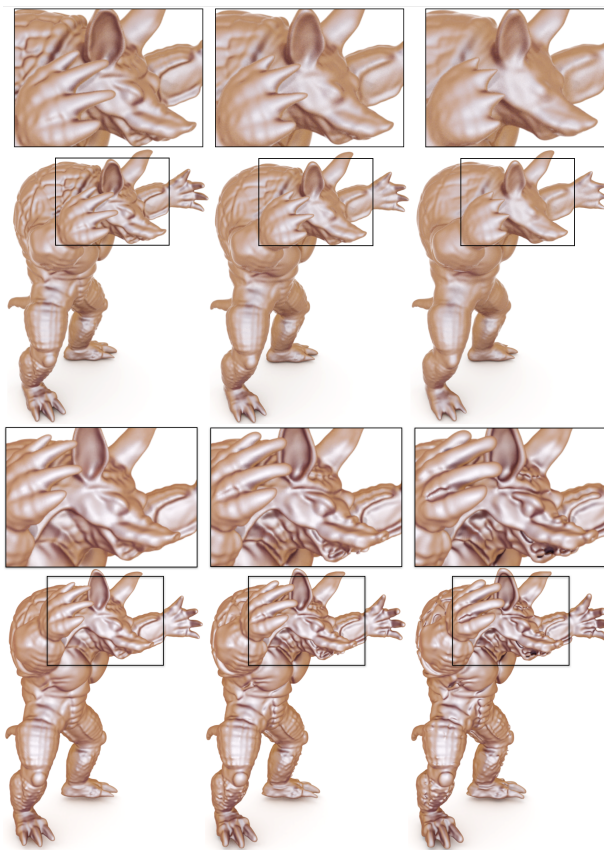


Figure 15: Smoothing and Sharpening the Armadillo with the method from Novello et al. [35].

different expressions of the same face. In this context, Zheng et al. [73] proposes to leverage INRs by creating expression and identity deformations between previously captured faces. They expand on DeepSDF [37], and create two separate latent spaces: one for expressions, and one for identities. A third network encodes a template shape, which is the average face of the dataset. The authors further expanded their method by incorporating a refined displacement grid to capture finer facial details [74]. Both works incorporate the Eikonal term as a regularizer for the loss function in addition to a normal alignment term. Using a separate network for the flow, as done in another domain in Schardong et al. [44], holds promise



Figure 16: Deformation and interpolation of INRs. Top row shows the evolution of the zero-level sets of an INR according to a vector field with a source and a sink. The SDF of the Spot is the initial condition at $t = 0$ (middle). The sink/source is inside the head/body of the Spot. Bottom row shows an example of shape interpolation between Bob, positioned at $t = 0$ and Spot, at $t = 1$. Images adapted from [35].

for this field.

Wang et al. [59] expands NeuS [58] to dynamic scene reconstruction from videos, by improving the training performance of NeuS with HashGrids introduced by InstantNGP [32]. They exploit a key property that the main object remains reasonably static on successive frames and propose an incremental training scheme from a base INR built from the first video frame. Additionally, they regularize their loss term using an Eikonal term, similarly to Novello et al. [34].

5 Conclusion

The paper reviewed INR approaches for solving the problem of implicit surface reconstruction by applying geometric regularization to the INR’s level sets. To present these approaches, we introduced a *geometric INR* framework, outlining a commonly used pipeline in this field. We defined the key components of this pipeline, including *input data*, which can consist of either oriented point clouds or posed images, and a *geometric loss function*, which leverages the differential properties of the function for regularization and sampling during training.

Additionally, we explored several applications that leverage the differentiability of neural networks and the discrete geometry of oriented point clouds to fit the INR’s zero-level set to the data. Our review covers prominent geometric INRs, such as SIREN and IGR, along with state-of-the-art methods from image-based reconstruction literature, like NeuS and Neuralangelo. These methods demonstrate that incorporating differential geometry concepts into the INR loss function offers significant potential for reconstructing surfaces from posed images.

References

- [1] Dejan Azinović, Ricardo Martin-Brualla, Dan B Goldman, Matthias Nießner, and Justus Thies. Neural rgb-d surface reconstruction. In *Proceedings of the IEEE/CVF Conference on Computer Vision and Pattern Recognition*, pages 6290–6301, 2022.
- [2] Jonathan T Barron, Ben Mildenhall, Matthew Tancik, Peter Hedman, Ricardo Martin-Brualla, and Pratul P Srinivasan. Mip-nerf: A multiscale representation for anti-aliasing neural radiance fields. In *Proceedings of the IEEE/CVF international conference on computer vision*, pages 5855–5864, 2021.
- [3] Jonathan C Carr, Richard K Beatson, Jon B Cherrie, Tim J Mitchell, W Richard Fright, Bruce C McCallum, and Tim R Evans. Reconstruction and representation of 3d objects with radial basis functions. In *Proceedings of the 28th annual conference on Computer graphics and interactive techniques*, pages 67–76, 2001.
- [4] Yinbo Chen, Sifei Liu, and Xiaolong Wang. Learning continuous image representation with local implicit image function. In *Proceedings of the IEEE/CVF conference on computer vision and pattern recognition*, pages 8628–8638, 2021.
- [5] Vinícius da Silva, Tiago Novello, Guilherme Schardong, Luiz Schirmer, Hélio Lopes, and Luiz Velho. Mip-plicits: Level of detail factorization

- of neural implicits sphere tracing. *arXiv preprint arXiv:2201.09147*, 2, 2022.
- [6] François Darmon, Bénédicte Bascle, Jean-Clément Devaux, Pascal Monasse, and Mathieu Aubry. Improving neural implicit surfaces geometry with patch warping. In *Proceedings of the IEEE/CVF Conference on Computer Vision and Pattern Recognition*, pages 6260–6269, 2022.
- [7] Akshat Dave, Yongyi Zhao, and Ashok Veeraraghavan. Pandora: Polarization-aided neural decomposition of radiance. In *European Conference on Computer Vision*, pages 538–556. Springer, 2022.
- [8] Miguel Fainstein, Viviana Siless, and Emmanuel Iarussi. Dufd: Differentiable unsigned distance fields with hyperbolic scaling. In *Proceedings of the IEEE/CVF Conference on Computer Vision and Pattern Recognition*, pages 4484–4493, 2024.
- [9] Martin A Fischler and Robert C Bolles. Random sample consensus: a paradigm for model fitting with applications to image analysis and automated cartography. *Communications of the ACM*, 24(6):381–395, 1981.
- [10] Qiancheng Fu, Qingshan Xu, Yew Soon Ong, and Wenbing Tao. Geo-neus: Geometry-consistent neural implicit surfaces learning for multi-view reconstruction. *Advances in Neural Information Processing Systems*, 35:3403–3416, 2022.
- [11] Amos Gropp, Lior Yariv, Niv Haim, Matan Atzmon, and Yaron Lipman. Implicit geometric regularization for learning shapes. In *Proceedings of the 37th International Conference on Machine Learning*, ICML’20. JMLR.org, 2020.
- [12] John C Hart. Sphere tracing: A geometric method for the antialiased ray tracing of implicit surfaces. *The Visual Computer*, 12(10):527–545, 1996.
- [13] Rasmus Jensen, Anders Dahl, George Vogiatzis, Engin Tola, and Henrik Aanæs. Large scale multi-view stereopsis evaluation. In *Proceedings of the IEEE conference on computer vision and pattern recognition*, pages 406–413, 2014.
- [14] Yining Jiao, Carlton Jude ZDANSKI, Julia S Kimbell, Andrew Prince, Cameron P Worden, Samuel Kirse, Christopher Rutter, Benjamin Shields, William Alexander Dunn, Jisan Mahmud, and Marc Niethammer. NAISR: A 3d neural additive model for interpretable shape representation. In *The Twelfth International Conference on Learning Representations*, 2024. URL <https://openreview.net/forum?id=wg8NPfeMF9>.
- [15] James T Kajiya and Brian P Von Herzen. Ray tracing volume densities. *ACM SIGGRAPH computer graphics*, 18(3):165–174, 1984.
- [16] Michael Kazhdan, Matthew Bolitho, and Hugues Hoppe. Poisson surface reconstruction. In *Proceedings of the fourth Eurographics symposium on Geometry processing*, volume 7, 2006.
- [17] Arno Knapitsch, Jaesik Park, Qian-Yi Zhou, and Vladlen Koltun. Tanks and temples: Benchmarking large-scale scene reconstruction. *ACM Transactions on Graphics (ToG)*, 36(4):1–13, 2017.
- [18] Ruilong Li, Hang Gao, Matthew Tancik, and Angjoo Kanazawa. Nerfacc: Efficient sampling accelerates nerfs. In *Proceedings of the IEEE/CVF International Conference on Computer Vision*, pages 18537–18546, 2023.
- [19] Zhaoshuo Li, Thomas Müller, Alex Evans, Russell H Taylor, Mathias Unberath, Ming-Yu Liu, and Chen-Hsuan Lin. Neuralangelo: High-fidelity neural surface reconstruction. In *Proceedings of the IEEE/CVF Conference on Computer Vision and Pattern Recognition*, pages 8456–8465, 2023.
- [20] David B Lindell, Dave Van Veen, Jeong Joon Park, and Gordon Wetzstein. Bacon: Band-limited coordinate networks for multiscale scene representation. In *Proceedings of the IEEE/CVF conference on computer vision and pattern recognition*, pages 16252–16262, 2022.

- [21] Xiaoxiao Long, Cheng Lin, Peng Wang, Taku Komura, and Wenping Wang. Sparseneus: Fast generalizable neural surface reconstruction from sparse views. In *European Conference on Computer Vision*, pages 210–227. Springer, 2022.
- [22] William E Lorensen and Harvey E Cline. Marching cubes: A high resolution 3d surface construction algorithm. In *Seminal graphics: pioneering efforts that shaped the field*, pages 347–353. ACM, 1998.
- [23] David G Lowe. Object recognition from local scale-invariant features. In *Proceedings of the seventh IEEE international conference on computer vision*, volume 2, pages 1150–1157. Ieee, 1999.
- [24] Baorui Ma, Junsheng Zhou, Yu-Shen Liu, and Zhizhong Han. Towards better gradient consistency for neural signed distance functions via level set alignment. In *Proceedings of the IEEE/CVF Conference on Computer Vision and Pattern Recognition*, pages 17724–17734, 2023.
- [25] Stephane G Mallat. A theory for multiresolution signal decomposition: the wavelet representation. *IEEE transactions on pattern analysis and machine intelligence*, 11(7):674–693, 1989.
- [26] Zoë Marschner, Silvia Sellán, Hsueh-Ti Derek Liu, and Alec Jacobson. Constructive solid geometry on neural signed distance fields. In *SIGGRAPH Asia 2023 Conference Papers*, pages 1–12, 2023.
- [27] Nelson Max. Optical models for direct volume rendering. *IEEE Transactions on Visualization and Computer Graphics*, 1(2):99–108, 1995.
- [28] Boris Mederos, Luiz Velho, and Luiz Henrique De Figueiredo. Moving least squares multiresolution surface approximation. In *16th Brazilian symposium on computer graphics and image processing (SIBGRAPI 2003)*, pages 19–26. IEEE, 2003.
- [29] Ishit Mehta, Manmohan Chandraker, and Ravi Ramamoorthi. A level set theory for neural implicit evolution under explicit flows. In *European Conference on Computer Vision*, pages 711–729. Springer, 2022.
- [30] Lars Mescheder, Michael Oechsle, Michael Niemeyer, Sebastian Nowozin, and Andreas Geiger. Occupancy networks: Learning 3d reconstruction in function space. In *Proceedings of the IEEE/CVF conference on computer vision and pattern recognition*, pages 4460–4470, 2019.
- [31] Ben Mildenhall, Pratul P Srinivasan, Matthew Tancik, Jonathan T Barron, Ravi Ramamoorthi, and Ren Ng. Nerf: Representing scenes as neural radiance fields for view synthesis. In *European conference on computer vision*, pages 405–421. Springer, 2020.
- [32] Thomas Müller, Alex Evans, Christoph Schied, and Alexander Keller. Instant neural graphics primitives with a multiresolution hash encoding. *ACM transactions on graphics (TOG)*, 41(4):1–15, 2022.
- [33] Michael Niemeyer, Lars Mescheder, Michael Oechsle, and Andreas Geiger. Occupancy flow: 4d reconstruction by learning particle dynamics. In *2019 IEEE/CVF International Conference on Computer Vision (ICCV)*, pages 5378–5388, 2019. doi: 10.1109/ICCV.2019.00548.
- [34] Tiago Novello, Guilherme Schardong, Luiz Schirmer, Vinicius da Silva, Helio Lopes, and Luiz Velho. Exploring differential geometry in neural implicit. *Computers & Graphics*, 108: 49–60, 2022.
- [35] Tiago Novello, Vinicius da Silva, Guilherme Schardong, Luiz Schirmer, Helio Lopes, and Luiz Velho. Neural implicit surface evolution. In *Proceedings of the IEEE/CVF International Conference on Computer Vision*, pages 14279–14289, 2023.

- [36] Michael Oechsle, Songyou Peng, and Andreas Geiger. Unisurf: Unifying neural implicit surfaces and radiance fields for multi-view reconstruction. In *International Conference on Computer Vision (ICCV)*, 2021.
- [37] Jeong Joon Park, Peter Florence, Julian Straub, Richard Newcombe, and Steven Lovegrove. DeepSDF: Learning continuous signed distance functions for shape representation. In *Proceedings of the IEEE/CVF Conference on Computer Vision and Pattern Recognition*, pages 165–174, 2019.
- [38] Hallison Paz, Tiago Novello, Vinicius Silva, Luiz Schirmer, Guilherme Schardong, Fabio Chagas, Helio Lopes, and Luiz Velho. Multiresolution neural networks for imaging. In *Proceedings of 35th Conference on Graphics, Patterns and Images (SIBGRAPI)*, 2022. to appear.
- [39] Hallison Paz, Daniel Perazzo, Tiago Novello, Guilherme Schardong, Luiz Schirmer, Vinicius da Silva, Daniel Yukimura, Fabio Chagas, Helio Lopes, and Luiz Velho. Mr-net: Multiresolution sinusoidal neural networks. *Computers & Graphics*, 2023.
- [40] Hallison Paz, Tiago Novello, and Luiz Velho. Implicit neural representation of tileable material textures. *arXiv preprint arXiv:2402.02208*, 2024.
- [41] Daniel Perazzo, João Paulo Lima, Luiz Velho, and Veronica Teichrieb. Directvoxgo++: Grid-based fast object reconstruction using radiance fields. *Computers & Graphics*, 114:96–104, 2023.
- [42] Lu Sang, Abhishek Saroha, Maolin Gao, and Daniel Cremers. Enhancing surface neural implicits with curvature-guided sampling and uncertainty-augmented representations, 2023. URL <https://arxiv.org/abs/2306.02099>.
- [43] Vishwanath Saragadam, Jasper Tan, Guha Balakrishnan, Richard G Baraniuk, and Ashok Veeraraghavan. Miner: Multiscale implicit neural representation. In *European Conference on Computer Vision*, pages 318–333. Springer, 2022.
- [44] Guilherme Schardong, Tiago Novello, Hallison Paz, Iurii Medvedev, Vinicius da Silva, Luiz Velho, and Nuno Gonçalves. Neural implicit morphing of face images, 2024.
- [45] Luiz Schirmer, Guilherme Schardong, Vinicius da Silva, Hélio Lopes, Tiago Novello, Daniel Yukimura, Thales Magalhaes, Hallison Paz, and Luiz Velho. Neural networks for implicit representations of 3d scenes. In *2021 34th SIBGRAPI Conference on Graphics, Patterns and Images (SIBGRAPI)*, pages 17–24. IEEE, 2021.
- [46] Luiz Schirmer, Tiago Novello, Guilherme Schardong, Vinicius da Silva, Hélio Lopes, and Luiz Velho. How to train your (neural) dragon. In *Conference on Graphics, Patterns and Images*, 2023. URL <http://urlib.net/ibi/8JMKD3MGPEW34M/49T46US>.
- [47] Johannes Lutz Schönberger and Jan-Michael Frahm. Structure-from-motion revisited. In *Conference on Computer Vision and Pattern Recognition (CVPR)*, 2016.
- [48] Akhmedkhan Shabanov, Shrisudhan Govindarajan, Cody Reading, Lily Goli, Daniel Rebain, Kwang Moo Yi, and Andrea Tagliasacchi. Banf: Band-limited neural fields for levels of detail reconstruction. In *Proceedings of the IEEE/CVF Conference on Computer Vision and Pattern Recognition*, pages 20571–20580, 2024.
- [49] Vincent Sitzmann, Julien Martel, Alexander Bergman, David Lindell, and Gordon Wetzstein. Implicit neural representations with periodic activation functions. *Advances in Neural Information Processing Systems*, 33, 2020.
- [50] Pratul P Srinivasan, Ben Mildenhall, Matthew Tancik, Jonathan T Barron, Richard Tucker, and Noah Snavely. Lighthouse: Predicting lighting volumes for spatially-coherent illumination. In *Proceedings of the IEEE/CVF Conference on Computer Vision and Pattern Recognition*, pages 8080–8089, 2020.

- [51] Peder Bergebakken Sundt and Theoharis Theoharis. Marf: The medial atom ray field object representation. *Computers & Graphics*, 115:122–136, 2023.
- [52] Richard Szeliski. *Computer vision: algorithms and applications*. Springer Nature, 2022.
- [53] Towaki Takikawa, Joey Litalien, Kangxue Yin, Karsten Kreis, Charles Loop, Derek Nowrouzezahrai, Alec Jacobson, Morgan McGuire, and Sanja Fidler. Neural geometric level of detail: Real-time rendering with implicit 3d shapes. In *Proceedings of the IEEE/CVF Conference on Computer Vision and Pattern Recognition (CVPR)*, pages 11358–11367, June 2021.
- [54] Matthew Tancik, Pratul Srinivasan, Ben Mildenhall, Sara Fridovich-Keil, Nithin Raghavan, Utkarsh Singhal, Ravi Ramamoorthi, Jonathan Barron, and Ren Ng. Fourier features let networks learn high frequency functions in low dimensional domains. *Advances in neural information processing systems*, 33:7537–7547, 2020.
- [55] Matthew Tancik, Ethan Weber, Evonne Ng, Ruilong Li, Brent Yi, Justin Kerr, Terrance Wang, Alexander Kristoffersen, Jake Austin, Kamyar Salahi, Abhik Ahuja, David McAllister, and Angjoo Kanazawa. Nerfstudio: A modular framework for neural radiance field development. In *ACM SIGGRAPH 2023 Conference Proceedings*, SIGGRAPH '23, 2023.
- [56] Kushagra Tiwary, Akshat Dave, Nikhil Behari, Tzofi Klinghoffer, Ashok Veeraraghavan, and Ramesh Raskar. Orca: Glossy objects as radiance-field cameras. In *Proceedings of the IEEE/CVF Conference on Computer Vision and Pattern Recognition*, pages 20773–20782, 2023.
- [57] Shimon Ullman. The interpretation of structure from motion. *Proceedings of the Royal Society of London. Series B. Biological Sciences*, 203 (1153):405–426, 1979.
- [58] Peng Wang, Lingjie Liu, Yuan Liu, Christian Theobalt, Taku Komura, and Wenping Wang. Neus: Learning neural implicit surfaces by volume rendering for multi-view reconstruction. In M. Ranzato, A. Beygelzimer, Y. Dauphin, P.S. Liang, and J. Wortman Vaughan, editors, *Advances in Neural Information Processing Systems*, volume 34, pages 27171–27183. Curran Associates, Inc., 2021.
- [59] Yiming Wang, Qin Han, Marc Habermann, Kostas Daniilidis, Christian Theobalt, and Lingjie Liu. Neus2: Fast learning of neural implicit surfaces for multi-view reconstruction. In *Proceedings of the IEEE/CVF International Conference on Computer Vision*, pages 3295–3306, 2023.
- [60] Lance Williams. Pyramidal parametrics. In *Proceedings of the 10th annual conference on computer graphics and interactive techniques*, pages 1–11, 1983.
- [61] Guandao Yang, Serge Belongie, Bharath Hariharan, and Vladlen Koltun. Geometry processing with neural fields. *Advances in Neural Information Processing Systems*, 34:22483–22497, 2021.
- [62] Lior Yariv, Yoni Kasten, Dror Moran, Meirav Galun, Matan Atzmon, Basri Ronen, and Yaron Lipman. Multiview neural surface reconstruction by disentangling geometry and appearance. In H. Larochelle, M. Ranzato, R. Hadsell, M.F. Balcan, and H. Lin, editors, *Advances in Neural Information Processing Systems*, volume 33, pages 2492–2502. Curran Associates, Inc., 2020.
- [63] Lior Yariv, Jiatao Gu, Yoni Kasten, and Yaron Lipman. Volume rendering of neural implicit surfaces. In M. Ranzato, A. Beygelzimer, Y. Dauphin, P.S. Liang, and J. Wortman Vaughan, editors, *Advances in Neural Information Processing Systems*, volume 34, pages 4805–4815. Curran Associates, Inc., 2021.
- [64] Lior Yariv, Peter Hedman, Christian Reiser, Dor Verbin, Pratul P Srinivasan, Richard

- Szeliski, Jonathan T Barron, and Ben Mildenhall. Baked sdf: Meshing neural sdf for real-time view synthesis. In *ACM SIGGRAPH 2023 Conference Proceedings*, pages 1–9, 2023.
- [65] Wang Yifan, Lukas Rahmann, and Olga Sorkine-Hornung. Geometry-consistent neural shape representation with implicit displacement fields. *arXiv preprint arXiv:2106.05187*, 2021.
- [66] Alex Yu, Vickie Ye, Matthew Tancik, and Angjoo Kanazawa. pixelnerf: Neural radiance fields from one or few images. In *Proceedings of the IEEE/CVF conference on computer vision and pattern recognition*, pages 4578–4587, 2021.
- [67] Zehao Yu, Anpei Chen, Bozidar Antic, Songyou Peng, Apratim Bhattacharyya, Michael Niemeyer, Siyu Tang, Torsten Sattler, and Andreas Geiger. Sdfstudio: A unified framework for surface reconstruction, 2022. URL <https://github.com/autonomousvision/sdfstudio>.
- [68] Zehao Yu, Songyou Peng, Michael Niemeyer, Torsten Sattler, and Andreas Geiger. Monosdf: Exploring monocular geometric cues for neural implicit surface reconstruction. *Advances in neural information processing systems*, 35: 25018–25032, 2022.
- [69] Kai Zhang, Gernot Riegler, Noah Snavely, and Vladlen Koltun. Nerf++: Analyzing and improving neural radiance fields. *arXiv preprint arXiv:2010.07492*, 2020.
- [70] Kai Zhang, Fujun Luan, Qianqian Wang, Kavita Bala, and Noah Snavely. Physg: Inverse rendering with spherical gaussians for physics-based material editing and relighting. In *Proceedings of the IEEE/CVF Conference on Computer Vision and Pattern Recognition*, pages 5453–5462, 2021.
- [71] Xiuming Zhang, Pratul P Srinivasan, Boyang Deng, Paul Debevec, William T Freeman, and Jonathan T Barron. Nerfactor: Neural factorization of shape and reflectance under an unknown illumination. *ACM Transactions on Graphics (ToG)*, 40(6):1–18, 2021.
- [72] Fuqiang Zhao, Yuheng Jiang, Kaixin Yao, Jiakai Zhang, Liao Wang, Haizhao Dai, Yuhui Zhong, Yingliang Zhang, Minye Wu, Lan Xu, et al. Human performance modeling and rendering via neural animated mesh. *ACM Transactions on Graphics (TOG)*, 41(6):1–17, 2022.
- [73] Mingwu Zheng, Hongyu Yang, Di Huang, and Liming Chen. Imface: A nonlinear 3d morphable face model with implicit neural representations. In *Proceedings of the IEEE/CVF Conference on Computer Vision and Pattern Recognition*, pages 20343–20352, 2022.
- [74] Mingwu Zheng, Haiyu Zhang, Hongyu Yang, Liming Chen, and Di Huang. Imface++: A sophisticated nonlinear 3d morphable face model with implicit neural representations. *arXiv preprint arXiv:2312.04028*, 2023.